EFFECTS OF MICRO-HYDRATION IN PROTON TRANSFER FROM H₂S·NO⁺ COMPLEX TO WATER: *ab initio* AND MOLECULAR DYNAMICS STUDY

Ivan ČERNUŠÁK[a],*, Jozef FEDERIČ[a], Pavel JUNGWIRTH[b] and Milan UHLÁR[c]

[a] *Department of Physical and Theoretical Chemistry, Faculty of Natural Sciences, Comenius University, 842 15 Bratislava, Slovakia; e-mail: cernusak@fns.uniba.sk*

[b] *Institute of Organic Chemistry and Biochemistry, Academy of Sciences of the Czech Republic, v.v.i. and Center for Biomolecules and Complex Molecular Systems, 166 10 Prague 6, Czech Republic; e-mail: pavel.jungwirth@uochb.cas.cz*

[c] *Institute of Physics, Faculty of Philosophy and Science, Silesian University, Bezručovo nám. 13, 746 01 Opava 1, Czech Republic; e-mail: milan.uhlar@fpf.slu.cz*

Dedicated to Dr. Zdeněk Havlas on the occasion of his 60th birthday.

We have studied several microhydrated $(H_2O)_n \cdot NO^+ \cdot H_2S$ structures ($n = 1$–3) and their fragments using wave-function based approach (coupled-clusters including single, double and non-iterative triple substitutions – CCSD(T) and second-order perturbation theory – MP2) and also employing density functional theory (with BLYP and ωB97XD functional). MP2 energetics is very close to CCSD(T) one. Both functionals provide reasonable binding energies compared to MP2, the ωB97XD being superior to BLYP. The exploratory *ab initio* molecular dynamics performed on four- and five-body clusters revealed that the hydrogen bonds network and cooperativity in these systems play a crucial role in the proton transfer from $H_2S \cdot NO^+$ to H_2O and its conversion to thionitrous acid.

Keywords: *Ab initio* calculations; Atmospheric chemistry; Hydrogen bonds; Molecular dynamics.

Hydrogen bonding and proton transfer reactions are fascinating and important phenomena governing chemical and biological processes in polar solvents, biomolecules, and various molecular complexes[1–4]. Proton transfer is critical also in modelling the atmospheric reactions where the microhydration takes place. Crucial question associated with these phenomena is the origin of the driving force facilitating the proton transfer and closely related notion of the cooperativity in hydrogen bonded network[1,5]. The latter effect of non-additivity is typical for a string of H-bonds, resulting in stron-

ger binding between the members of a chain than would occur in individual H-bonds. This string may be both linear sequence or a ring and an important factor influencing the H-bond strength is the polarizability along the chain[6,7]. In this paper, we will investigate the intermolecular proton transfer in the title reaction focusing on the details of the overall process of the formation of a hydrogen bonded complex and the separation of the products.

Atmospheric chemistry involves variety of gaseous species – inorganic oxides, oxidants, reductants, acids, bases, organics, photochemically active species and unstable intermediates (ions and electron excited molecules)[8,9]. Solid and liquid particles can form atmospheric aerosols and affect atmospheric chemistry of gas-phase species, either as sites for surface reactions or for processes in liquid droplets. The size of these species can range from aggregates of few molecules to larger nano-structures. In our considerations, we shall focus on the upper stratosphere. One of the important constituents of the upper stratosphere in altitudes around 20–50 km is the nitrogen oxide (NO) and its cation. Both NO and NO^+ belong to the most toxic pollutants in the atmosphere, affecting the ozone cycle and being a precursor of the acid rain. NO is present in the atmosphere mostly as a result of combustions by two mechanisms: (i) oxidation of the organic nitrogen of the fuel and (ii) combination of atmospheric nitrogen with oxygen at high temperature and pressure (in the internal combustion engine of automobiles). NO is produced in large quantities by both of these reactions, and emitted into the atmosphere. It is interesting that while NO is a minor constituent in the stratosphere, the NO^+ is a major one. This is due to the UV and particle impact that initiates chain of ion-molecule reactions at this altitude[10]. These ion-molecule reactions can also be enriched by the propagation of other molecules coming from the upper troposphere as a result of either human (industrial) activity or as a consequence of the processes of tropospheric origin that can perturb the stratosphere[11].

Based on previous studies[12–16], Mack, Dyke and Wright have analyzed the model of switching reactions between NO^+ and N_2, CO_2, and H_2O [17] at low temperatures. They have shown, on thermodynamic grounds, that the conversion from nude NO^+ ion to the monohydrated $NO^+ \cdot H_2O$ is feasible via intermediates $NO^+ \cdot N_2$ and $NO^+ \cdot CO_2$. In this scheme NO^+ prefers first to associate with the nitrogen molecule, due to large relative abundance of N_2. Once the complex NO^+ with N_2 has been formed, the switching reaction with CO_2 can take place. This step is favoured due to the relatively higher abundance of CO_2 compared to H_2O. Finally, the complex $NO^+ \cdot CO_2$ can re-

act with H_2O to give $NO^+ \cdot H_2O$. Closely related are the studies by Hiraoka and Yamabe[18] and Choi et al.[19] who have shown that NO^+ can form also larger clusters with more ligands (typically up to 3) in the D region of the Earth atmosphere. Note that the D region overlaps largely with the mesosphere (ranging approximately from 50 to 90 km above the Earth). In the latter paper authors also demonstrated that there is a possible reaction channel, intra cluster reaction $NO^+ \cdot (H_2O)_{n-1} + H_2O \rightarrow H_3O^+(H_2O)_{n-2} +$ HONO, accompanied by the charge transfer from nitrogen atom to H_3O^+ moiety. This intra-cluster reaction is best promoted (exothermic) for $n = 5$, but can proceed as slightly endothermic also for $n = 4$. Recently, Asada, Nagaoka and Koseki combined *ab initio* molecular orbital calculations and molecular dynamics simulations[20] for the same system and confirmed that excess hydration binding energies for $n = 4$ and 5 facilitate surpassing the activation barriers towards HONO.

It is also generally accepted that small molecular clusters that include nitrogen oxide cation and other neutral ligands are plausible on the boundary between troposphere and stratosphere[12,13,16–19,21–29]. One of them, hydrogen sulfide (H_2S) can penetrate from the troposphere to the stratosphere due to organic matter decomposition, elevated volcanic activity (often in large quantities prior to an eruption) and/or industrial pollution[30–33]. Large explosive eruptions can inject a tremendous volume of sulfur aerosols into the stratosphere that can affect both the surface temperatures and the Earth ozone layer. The role of volcanic H_2S can become important when more abundant and reactive species in this region (e.g., OH, HO_2) are consumed by reaction with other volcanic gases SO_2 and HCl[31] and H_2S can persist in the atmosphere for tens of minutes[34]. Thus, at certain climatic conditions the interaction of atmospheric NO^+ with H_2S is possible. Other, although exotic option, is the interaction of NO/NO^+ with H_2S originating from the penetration of large meteorite into atmosphere at hypersonic velocities suggested by Hochstim in early 60ties[35].

Chemistry of atmospheric sulfur is still poorly understood, compared to carbon, oxygen or nitrogen[9]. The possible sulfur species are most abundant oxidized forms SO_2, SO_3 (with their precursors COS and CS_2) and reduced forms H_2S, $(CH_3)_2S$, $(CH_3)_2S_2$. Among them, H_2S may have lifetimes ranging from few minutes to few hours. According to Wayne, the mechanism of H_2S destruction is uncertain and may involve oxidation steps involving predominantly OH[9]. If the OH radical is effectively removed by competing reactions as noted in previous paragraph, one has to consider other species that can be of importance. Based on the rich atmospheric chemistry of the

nitric oxide cation (NO^+)[36] we propose an alternative way of H_2S destruction with the participation of NO^+. The underlying steps of this process are: 1) the formation of the $NO^+\cdot H_2S$ cluster; 2) its micro-hydration and 3) conversion of the hydrated cluster to HSNO and $H^+\cdot[H_2O]_n$ via the proton transfer from H_2S to the closest proton acceptor – H_2O molecule bound to H_2S through the hydrogen bond. The first two stages of this process were studied elsewhere[37,38]. In lit.[37] we have studied the thermodynamic stability of various naked $NO^+\cdot H_2S$ isomers, while in lit.[38] we have shown that two hydrogen-bonded water molecules in suitable geometry can promote the proton transfer from H_2S to NO^+ resulting in HSNO formation. We have also found that BLYP and MP2 barriers for this transfer are below 5 kJ mol^{-1}.

In this paper, we will focus on the comparison of the energetics of various hydrated $NO^+\cdot H_2S$ clusters and related fragments computed from density functional theory (DFT), using functionals BLYP [39–41] and ωB97XD [42,43], as well as from the high-level wave-functions methods – the second order perturbation theory (MP2)[44] and the coupled cluster theory including single, double and non-iterative triple substitutions (CCSD(T))[45–47].

Some of the hydrated $NO^+\cdot H_2S$ clusters were examined in our previous paper[38], the main focus of the present work is on four- and five-body clusters and some smaller fragments not investigated previously.

We also report our first attempts to simulate the time evolution of the conversion for the micro-hydration of $NO^+\cdot H_2S\cdot(H_2O)_n$ clusters with $n = 2$ and 3 using the DFT-CP molecular dynamics in [NVE] ensemble employing BLYP functional.

COMPUTATIONAL METHODS

Ab initio and DFT molecular calculations were performed using the ACES-II [48] and Gaussian 09 [49] codes. All geometry optimizations of the hydrated $NO^+\cdot H_2S$ clusters and their appropriate fragments were performed using the cc-pVTZ basis set[50]. Two types of hydrated clusters were investigated: four-body $NO^+\cdot H_2S\cdot(H_2O)_2$ and five-body $NO^+\cdot H_2S\cdot(H_2O)_3$. In addition, several cluster fragments that can be formed from these supermolecules were also calculated. In the DFT calculations, two functionals were employed: BLYP and ωB97XD. We have chosen the BLYP because in our subsequent CP-MD simulations we planned to exploit this functional. The choice of BLYP was dictated by its applicability in Car–Parrinello (CP) molecular dynamics[51].

ωB97XD is a hybrid functional introduced by Chai and Head–Gordon[42] and includes combination of long-range/short-range exchange and also empirical dispersion correction. The ωB97XD was chosen to test how it performs for the hydrogen-bonded complexes. It is supposed to be superior for dissociation and charge-transfer problems that are sensitive to self-interaction errors and we expect it to provide interaction energies closer to MP2 or CCSD(T). Our long term goal is to study systematically the dynamics of the complexation of the NO^+ ion with the series of hydrated atmospheric ligands, it is reasonable to perform the benchmark study with the aim to estimate the error bounds for both functionals in this particular type of complexes.
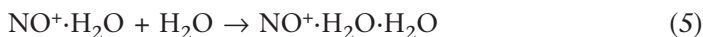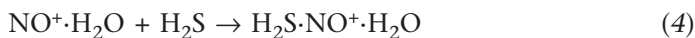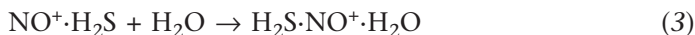
In the "standard" *ab initio* calculations we have adopted MP2 and CCSD(T) approaches. Since the CCSD(T) calculations are very demanding, only limited number of structures was optimized at this level. To convert the electronic energies to ΔH and ΔG we adopted standard ZPE and thermal corrections based on rigid-rotor/harmonic oscillator model for each level of approximation, except for CCSD(T) energies where MP2 corrections were used.

Following types of reactions have been considered in molecular cluster calculations (Tables I–III).

Association ion + ligand

$$NO^+ + H_2O \rightarrow NO^+ \cdot H_2O \tag{1}$$

$$NO^+ + H_2S \rightarrow NO^+ \cdot H_2S \tag{2}$$

Three-body cluster formation 2+1

$$NO^+ \cdot H_2S + H_2O \rightarrow H_2S \cdot NO^+ \cdot H_2O \tag{3}$$

$$NO^+ \cdot H_2O + H_2S \rightarrow H_2S \cdot NO^+ \cdot H_2O \tag{4}$$

$$NO^+ \cdot H_2O + H_2O \rightarrow NO^+ \cdot H_2O \cdot H_2O \tag{5}$$

Four-body cluster formation 2+2

$$H_2O \cdot H_2S + NO^+ \cdot H_2O \rightarrow H_2O \cdot H_2O \cdot H_2S \cdot NO^+ \tag{6}$$

$$H_2O \cdot H_2O + NO^+ \cdot H_2S \rightarrow H_2O \cdot H_2O \cdot H_2S \cdot NO^+ \tag{7}$$

Four-body cluster formation 3+1

$$H_2S \cdot NO^+ \cdot H_2O + H_2O \rightarrow H_2O \cdot H_2O \cdot H_2S \cdot NO^+ \tag{8}$$

$$NO^+ \cdot H_2O \cdot H_2O + H_2S \rightarrow H_2O \cdot H_2O \cdot H_2S \cdot NO^+ \tag{9}$$

$$H_2O \cdot H_2O \cdot H_2S + NO^+ \rightarrow H_2O \cdot H_2O \cdot H_2S \cdot NO^+ \tag{10}$$

Exchange H_2O/H_2S

$$NO^+ \cdot H_2O + H_2S \rightarrow NO^+ \cdot H_2S + H_2O \tag{11}$$

$$NO^+ \cdot H_2O \cdot H_2O + H_2S \rightarrow H_2S \cdot NO^+ \cdot H_2O + H_2O \tag{12}$$

Proton transfer

$$H_2O \cdot H_2O \cdot H_2S \cdot NO^+ \rightarrow H_2O \cdot [H_3O]^+ \cdot HS \cdot NO \tag{13}$$

Five-body cluster formation 4+1

$$H_2O \cdot H_2O \cdot H_2S \cdot NO^+ + H_2O \leftrightarrow (H_2O)_3 \cdot H_2S \cdot NO^+ \tag{14}$$

$$H_2O \cdot [H_3O]^+ \cdot HS \cdot NO + H_2O \leftrightarrow [H_7O_3]^+ \cdot HS \cdot NO \tag{15}$$
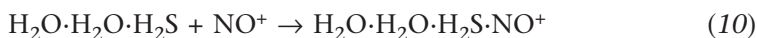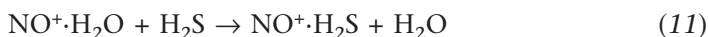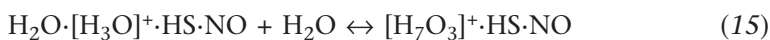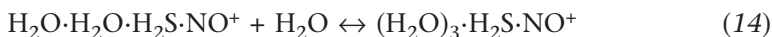
Ab initio molecular dynamics simulations in the microcanonical (NVE) ensemble were performed using the public domain computer code CP2K [52]. In its electronic structure module, DFT calculations are performed with the hybrid Gaussian and plane waves method (GPW)[53] and the electronic ground state density is self-consistently converged at each step (the so called Born–Oppenheimer dynamics). Kohn–Sham orbitals are expanded into atom-centred gaussian type orbital functions (triple-zeta quality – TZVP-MOLOPT-GTH [54]), while the electron density is represented with an auxiliary plane waves basis. Core electrons are removed by the introduction of norm conserving pseudopotentials developed by Goedecker, Teter and Hutter (GTH)[55]. As plane waves are intrinsically periodic, simulations of isolated systems are made possible with the introduction of a sufficiently large unit cell at least twice as large as the simulated system and the open boundary conditions

Poisson's solver[56]. Therefore, the water cluster was placed in the middle of a cubic box with a size of 20 × 20 × 20 Å. Simulations with the BLYP functional are more than an order of magnitude faster than those with the hybrid functionals, therefore, BLYP is usually the method of choice for small-to-medium sized clusters (few first-row atoms) for the time window spanning 10 ps, with a time step of 0.5 fs. This time window is sufficient for the charge-transport processes where low energy barriers are effectively washed out by zero-point motion[57–59].

RESULTS AND DISCUSSION

Prior to molecular cluster calculations we have scanned the two-dimensional cut through the MP2/cc-pVTZ potential energy surface (PES) of the $NO^+ \cdot H_2S \cdot (H_2O)_3$ cluster, $E = E(R_{OH}, R_{SH})$, keeping the remaining internal coordinates fixed at the optimal geometry of the five-body cluster (see insets in the top of Fig. 1). This scan shows the approximate energy landscape in the vicinity of the proton transfer illustrating the shallowness of the PES. It also indicates that one can expect the reverse reaction to proceed more easily than the forward one.
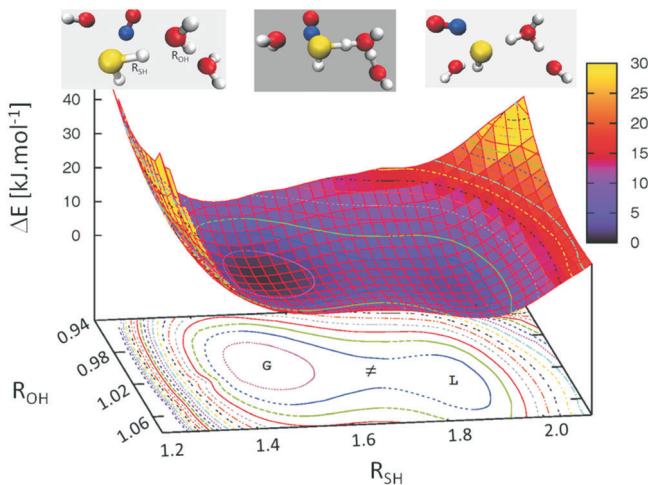

FIG. 1
2D-cut through the MP2/cc-pvTz potential energy hypersurface of the $NO^+ \cdot H_2S \cdot 3H_2O$ cluster. Surface represents the $E(R_{OH}, R_{SH})$ scan, all other internal coordinates were fixed. Structures G, ≠ and L are depicted as insets in the top of the Figure

Structures of the clusters are displayed in Figs 2 and 3. Cluster A refers to hydration of the $H_2S \cdot NO^+ \cdot H_2O$ with water dimer, cluster B refers to the attachment of the exo-water molecule to the four-membered quasi-ring $H_2O \cdot H_2O \cdot H_2S \cdot NO^+$, cluster C is the product after proton transfer – intermediate HSNO attached to Zundel structure $[H_7O_3]^+$. We use the term intermediate because the S⋯N bond is still rather elongated. Indeed, the subsequent dynamics showed that this structure is fragile and prone to dissociation, at least at the level of theory used in this work. This is in agreement with previous MRCI calculations of Nonella, Huber and Ha who have found that the isomer HNSO is more stable than HSNO [60].

$NO^+ \cdot H_2S$

$NO^+ \cdot H_2O$

$H_2O \cdot H_2S$

$H_2O \cdot H_2O$

$H_2S \cdot NO^+ \cdot H_2O$

$NO^+ \cdot H_2O \cdot H_2O$

$H_2O \cdot H_2O \cdot H_2S \cdot NO^+$ (a)

$H_2O \cdot H_2O \cdot H_2S \cdot NO^+$ (b)
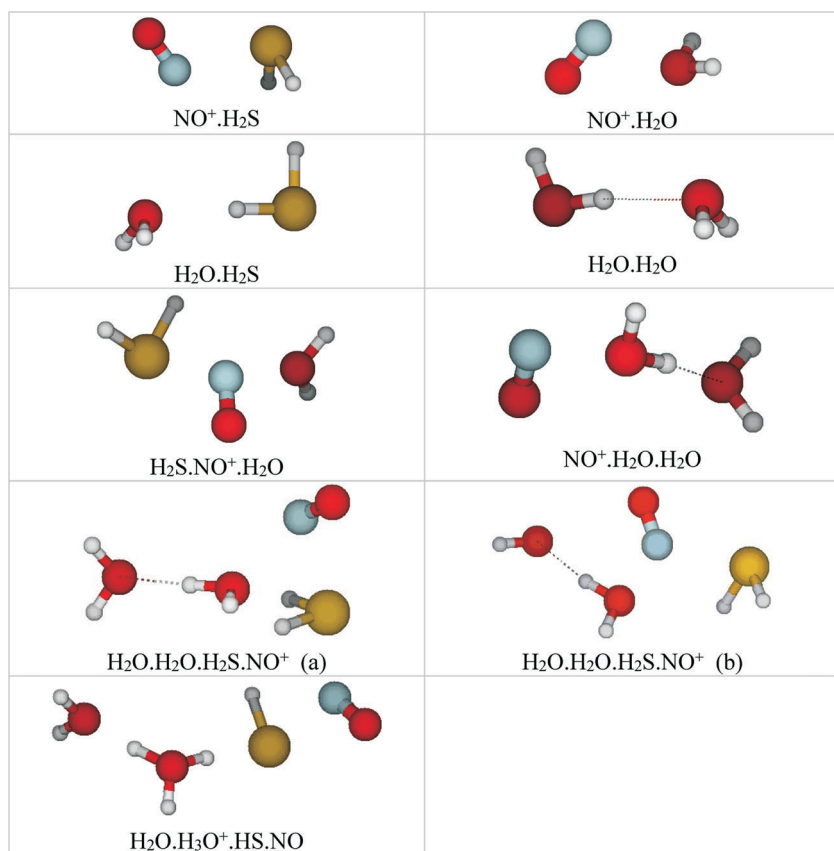
$H_2O \cdot H_3O^+ \cdot HS \cdot NO$

Fig. 2
Structures of two-, three- and four-body clusters

We have also located other similar five-body clusters but they differ from the structures A, B and C only slightly (both in terms of geometry and energy) and will not be discussed in detail. In Tables I–III we report the standard enthalpies and Gibbs energies at 200 K describing the process of gradual micro-hydration of the $H_2S \cdots NO^+$ complex and/or its fragments. We have chosen $T = 200$ K, this is the average temperature mimicking the
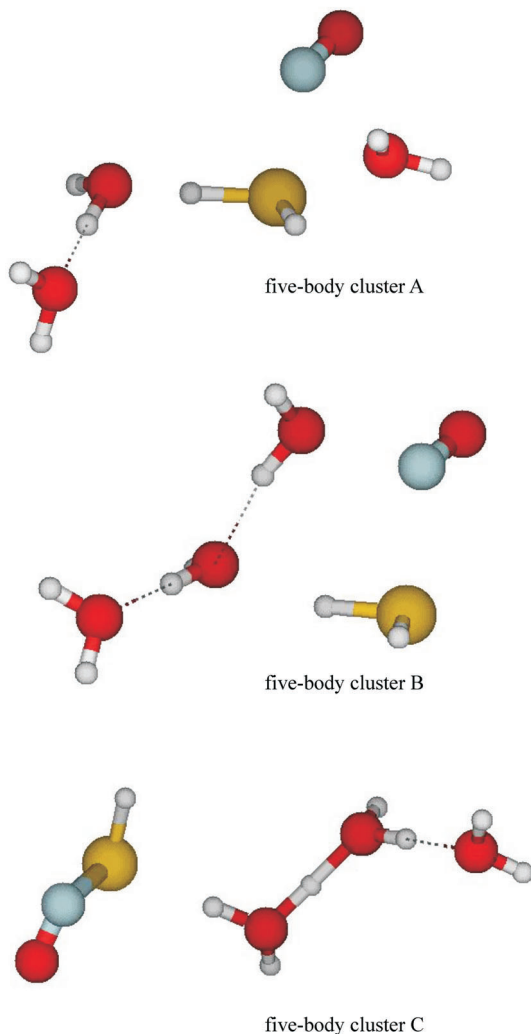

five-body cluster A

five-body cluster B

five-body cluster C

FIG. 3
Structures of the five-body clusters A, B and C

TABLE I
Comparison of BLYP, ωB97XD, MP2 and CCSD(T) thermodynamic quantities (kJ mol^{-1})

Process	BLYP		ωB97XD		MP2		CCSD(T)[a]	
	ΔH_{200K}	ΔG_{200K}	ΔH_{200K}	ΔG_{200K}	ΔH_{200K}	ΔG_{200K}	ΔH_{200K}	ΔG_{200K}
(1) $NO^+ + H_2O \rightarrow NO^+ \cdot H_2O$	-138.4	-118.3	-105.6	-85.6	-86.9	-65.5	-85.7	-64.3
(2) $NO^+ + H_2S \rightarrow NO^+ \cdot H_2S$	-159.6	-140.2	-107.5	-86.5	-78.2	-57.9	-76.1	-55.8
(3) $NO^+ \cdot H_2S + H_2O \rightarrow H_2S \cdot NO^+ \cdot H_2O$	-69.1	-41.8	-64.8	-38.7	-64.7	-38.4	-61.6	-35.4
(4) $NO^+ \cdot H_2O + H_2S \rightarrow H_2S \cdot NO^+ \cdot H_2O$	-90.3	-63.7	-66.7	-39.7	-56.0	-30.7	-52.1	-26.8
(5) $NO^+ \cdot H_2O + H_2O \rightarrow NO^+ \cdot H_2O \cdot H_2O$	-92.7	-66.3	-81.2	-55.6	-69.8	-47.3	-67.9	-45.4
(11) $NO^+ \cdot H_2O + H_2S \rightarrow NO^+ \cdot H_2S + H_2O$	-21.1	-21.9	-1.9	-0.9	8.7	7.7	9.6	8.6
(12) $NO^+ \cdot H_2O \cdot H_2O + H_2S \rightarrow H_2S \cdot NO^+ \cdot H_2O + H_2O$	2.4	2.5	14.5	15.9	13.8	16.6	15.8	18.6

[a] Using MP2 vibrational and thermal corrections.

TABLE II
Micro-solvation described by the BLYP and ωB97XD (kJ mol^{-1})

Process	BLYP		ωB97XD	
	ΔH_{200K}	ΔG_{200K}	ΔH_{200K}	ΔG_{200K}
(6) $H_2O \cdot H_2S + NO^+ \cdot H_2O \rightarrow H_2O \cdot H_2O \cdot H_2S \cdot NO^+$	−143.4	−110.8	−112.9	−81.3
(7) $H_2O \cdot H_2O + NO^+ \cdot H_2S \rightarrow H_2O \cdot H_2O \cdot H_2S \cdot NO^+$	−112.6	−79.8	−102.5	−73.5
(8) $H_2S \cdot NO^+ \cdot H_2O + H_2O \rightarrow H_2O \cdot H_2O \cdot H_2S \cdot NO^+$	−62.9	−40.5	−57.2	−36.6
(9) $NO^+ \cdot H_2O \cdot H_2O + H_2S \rightarrow H_2O \cdot H_2O \cdot H_2S \cdot NO^+$	−60.4	−38.0	−42.6	−20.7
(10) $H_2O \cdot H_2O \cdot H_2S + NO^+ \rightarrow H_2O \cdot H_2O \cdot H_2S \cdot NO^+$	−248.7	−225.8	−183.4	−161.0
(13) $H_2O \cdot H_2O \cdot H_2S \cdot NO^+ \rightarrow H_2O \cdot [H_3O]^+ \cdot HS \cdot NO$	−15.6	−14.3	−19.4	−16.5

stratospheric conditions during night. In Table I, we present the subset of reactions resulting in two- and three-body clusters, here we employed all four methods, BLYP, ωB97XD, MP2 and CCSD(T). In Tables II and III, we present the rest of the association reactions of larger clusters calculated only at BLYP and ωB97XD levels. Comparison of the MP2, BLYP and

TABLE III
Attachment of the third water molecule to four-body cluster. BLYP and ωB97XD thermodynamics (kJ mol^{-1})

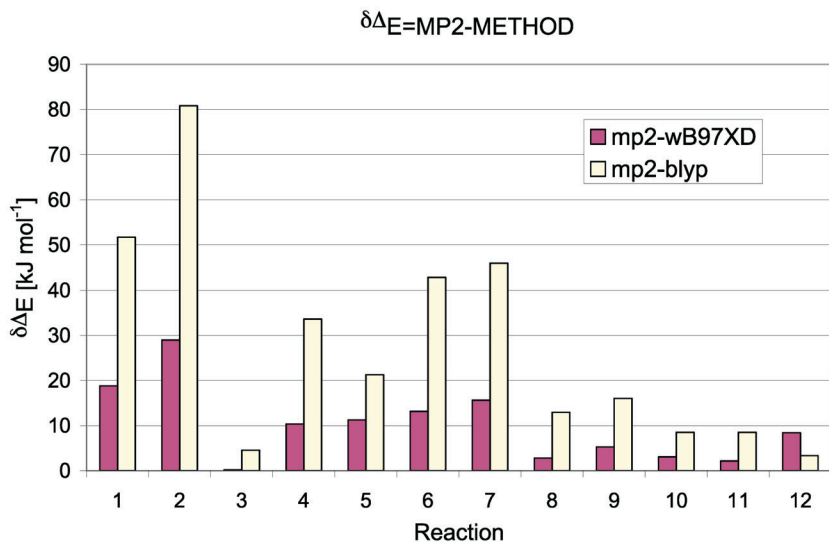| Process	BLYP		ωB97XD	
	ΔH_{200K}	ΔG_{200K}	ΔH_{200K}	ΔG_{200K}
(*14a*) $H_2O \cdot H_2O \cdot H_2S \cdot NO^+ + H_2O \leftrightarrow A$	−46.9	−23.3	−48.5	−24.3
(*14b*) $H_2O \cdot H_2O \cdot H_2S \cdot NO^+ + H_2O \leftrightarrow B$	−61.4	−33.3	−61.4	−31.6
(*14c*) $H_2O \cdot H_2O \cdot H_2S \cdot NO^+ + H_2O \leftrightarrow C$	−89.4	−67.2	−94.3	−72.6
(*15*) $H_2O \cdot [H_3O]^+ \cdot HS \cdot NO + H_2O \leftrightarrow C$	−91.3	−70.4	−75.0	−56.1

FIG. 4
Bar chart of the differences in reaction energies $\Delta E_{MP2} - \Delta E_{BLYP}$ and $\Delta E_{MP2} - \Delta E_{\omega B97XD}$ for reactions (*1*)–(*12*)

ωB97XD reaction energies is in Fig. 4 where we present differences MP2-BLYP and MP2-ωB97XD as a bar chart.

First, we can compare the MP2 and CCSD(T) energetics for a subset of reactions comprising smaller species, i.e., (1)–(5), (11) and (12). The MP2 reaction enthalpies and Gibbs energies are very close to CCSD(T) ones (Table I). In fact, the differences do not exceed ±4 kJ mol^{-1} which is conventionally accepted as chemical accuracy. This is not very surprising since this set includes either association/complexation processes or isodesmic reactions, for both the changes in correlation energies are expected to be small. Therefore, for the whole set of reactions we can use MP2 data as a reference. The performance of the ωB97XD functional proposed by Chai and Head–Gordon[42] is very good, while the differences observed for BLYP are substantially larger, especially for smaller systems. Yet the BLYP can describe the features of the energetics in reactions (1)–(12) qualitatively correctly. It is pleasing that as the systems' size grows the errors associated with BLYP tend to be smaller (Fig. 4). For reactions (8)–(11), all differences between MP2 and ωB97XD lie within 5 kJ mol^{-1} while the reaction (12) – proton transfer in four-body cluster – favours BLYP over ωB97XD.

Formation of two-, three-, four- and also five-body clusters is favoured thermodynamically (Tables I–III, Fig. 5) but there are variations depending on the way of their formation, size and degree of cooperativity in hydrogen
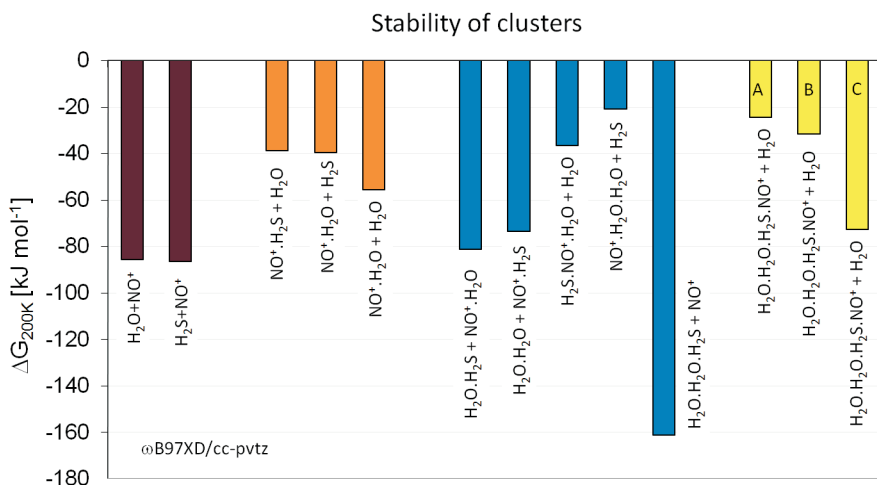

FIG. 5
Comparison of the thermodynamic stability of two-, three-, four- and five-body clusters calculated at ωB97XD/cc-pVTZ level

bonds. In Fig. 5, we compare ΔG_{200K} at ωB97XD/cc-pVTZ for various clusters of increasing size. Going from two- to three-body clusters (orange bars) is accompanied by slight increase of ΔG_{200K} (i.e., it becomes less negative), typical for attachment of the third particle to the two-body cluster. The cooperativity of hydrogen bonds takes place in four-body clusters (blue bars), most visible when the strongly polarizing NO^+ is attached to the sequential trimer $H_2O \cdot H_2O \cdot H_2S$ chain and less pronounced for the interaction of the solvated NO^+ with either $H_2O \cdot H_2O$ or $H_2O \cdot H_2S$ dimers. The relatively large (less negative) values of ΔG_{200K} in the case of clusters A and B result from the outermost position of one of the water molecules (in both these clusters). On the other hand, the presence of the sequential trimer $H_7O_3^+$ in structure C gives rise to moderate cooperativity effect associated with significant decrease in ΔG_{200K} (rightmost yellow bar in Fig. 5). The trends in Fig. 5 as well as the energetic in Tables I–III give also possible indications for the dynamics of the clusters in the atmosphere. The dissociation of NO^+ solvated with H_2O or H_2S ligands is thermodynamically not supported for two- or three-body cluster and NO^+ can be blocked in various solvated forms. However, once the favourable hydrogen-bonded chain of two or three water molecules is formed, with H_2O serving for H_2S as proton acceptor, the transfer of H^+ from H_2S to water cluster facilitates the formation of HSNO intermediate.

To shed more light on the dynamics we performed a few tens of CP-MD [NVE] simulations (lasting typically 10 ps) with slightly varying initial geometries based on the three-, four- and five-body clusters. All three-body and most of the four- and five-body trajectories were non-reactive. We have encountered reactive ones (e.g. with proton transfer and HSNO formation) only for those cases where the sequential hydrogen-bonded chain of two or three water molecules capped with H_2S was formed in the early stage of the simulation. Typical evolution of these model systems involving three four- and three five-body clusters are in Figs 6 and 7.

The top inset in Fig. 6 represents typical reactive collision of H_2S and H_2O where the proton-transfer occurs very early, within 0.1–0.2 ps. The red curve monitors the distance between oxygen atom of the proton acceptor and the hydrogen atom being transferred $R[O-H_S]$. Oscillations in $R[O-H_w]$ – H_w being the bridging hydrogen in $H_5O_2^+$ – are coupled with this motion (green curve). The middle inset in Fig. 6 shows shorter simulation with several attempts to push proton from H_2S to H_2O and simultaneous transfer of the second water molecules towards NO^+ resulting in nonreactive collision and effective blocking of NO^+ in the incomplete solvation cage. The bottom inset shows similar collision as in the top one but the resulting
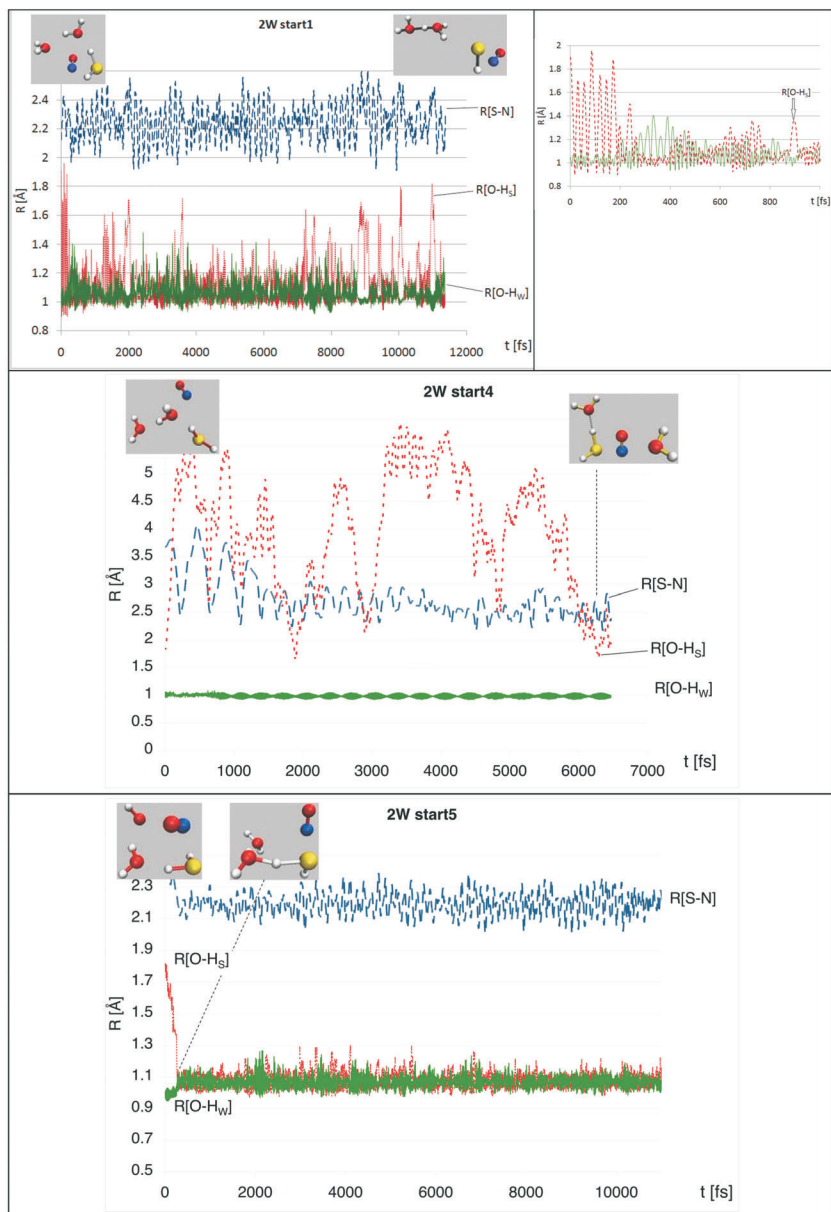
FIG. 6

Three typical trajectories in terms of geometry parameters for the NO$^+$·H$_2$S·2H$_2$O cluster from the [NVE] CP molecular dynamics. Top right inset displays the extended time scale from the beginning of the run in order to better notice the proton transfer (dashed line)
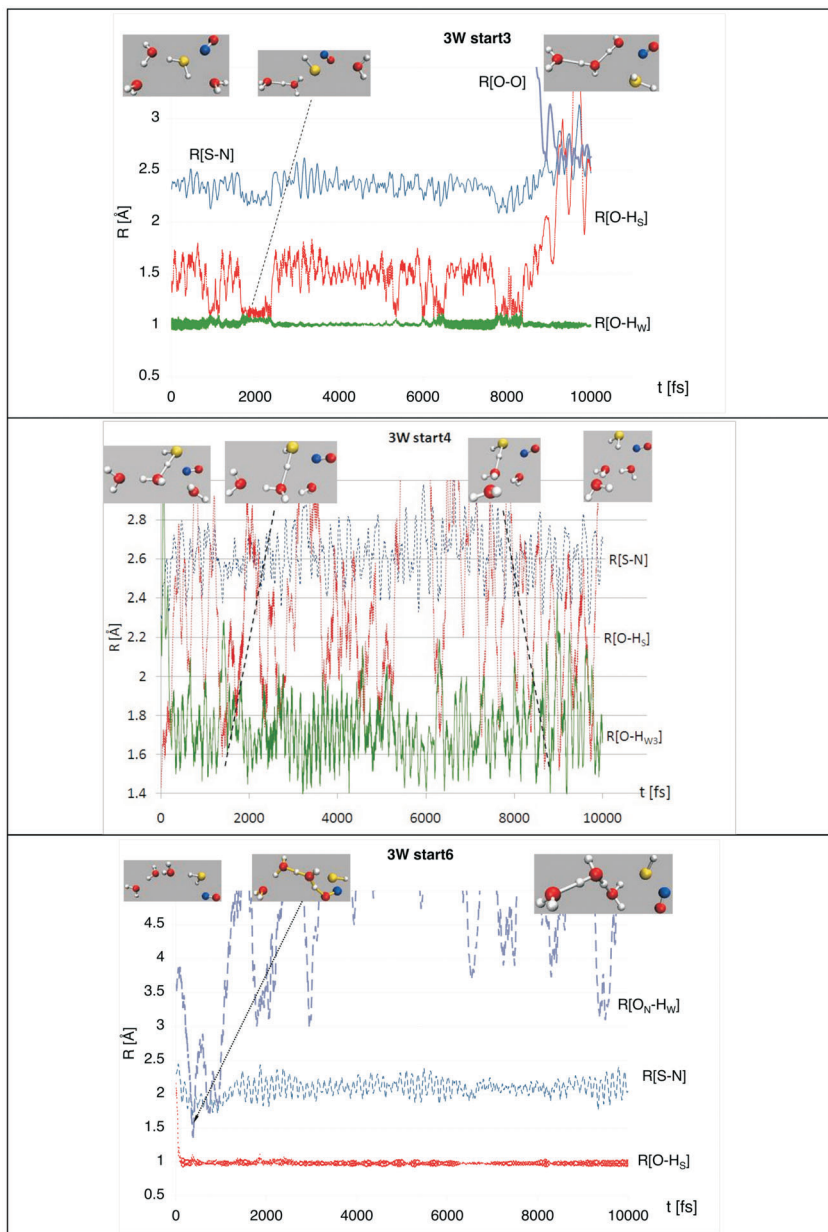
Three typical trajectories in terms of geometry parameters for the $NO^+ \cdot H_2S \cdot 3H_2O$ cluster from the [NVE] CP molecular dynamics

HSNO is more stable with smaller oscillation amplitude in R[S-N] and also R[O-H$_S$].

The top inset in Fig. 7 offers the MD trajectory with several proton transfers from H_2S to H_2O in the time span 8 ps accompanied with the transient formation of the N–S bond. After ~8–9 ps, H_2S is recombined due to the H_2O transfer originally coordinating NO$^+$ to water dimer preferring sequential trimer formation. Middle inset shows several attempts to promote the H-transfer, but there is apparent competition between H_2S and water molecule coordinating NO$^+$ which results in a compromise – build-up of the sequence $H_2S \cdot NO^+ \cdot (H_2O)_3$, the geometry that effectively blocks the proton transfer. The bottom inset represents typical reactive collision – the five-body cluster resembles bent linear chain in which the water molecules strongly cooperate and facilitate proton transfer in the early stage of the simulation. As an interesting feature (not observed in any other trajectory) one can see the transient formation of the $(H_2O)_2 \cdot H_3O^+ \cdot ONSH$ cluster that dissociates in within a picoseconds scale.

CONCLUSIONS

In this paper, we have investigated structures, energetic and dynamics of model system for solvated cation $H_2S \cdot NO^+$ interacting with 1–3 water molecules. We have shown that MP2/cc-pVTZ approach provides good benchmark binding energies that are very close to those obtained from the more demanding CCSD(T) method. The confrontation of BLYP and ωB97XD functionals confirmed that the latter provides better energetic for this type of complexes being in very good agreement with MP2 data for various types of hydration equilibria. Although the deviations in binding energies observed for BLYP are larger than for ωB97XD, the qualitative performance of the former functional is still acceptable for *ab initio* molecular dynamics. The results of the molecular dynamics simulations for four- and five-body clusters indicate that micro-solvation of $H_2S \cdot NO^+$ complex with 2–3 water molecules can promote almost barrier-less proton-transfer in the time window of few picoseconds and this process can lead to thionitrous acid.

REFERENCES

1. Scheiner S.: *Hydrogen bonding. A Theoretical Perspective*. Oxford University Press, New York 1997.
2. Schuster P., Wolschann P.: *Mon. Chem.* **1999**, *130*, 947.
3. Grabowski S. J. (Ed.): *Hydrogen Bonding – New Insights*, Vol. 3, p. 520. Springer Netherlands, Dordrecht 2006.
4. Hobza P., Havlas Z: *Theor. Chem. Acc.* **2002**, *108*, 325.
5. Mo O., Yanez M., Elguero J.: *J. Chem. Phys.* **1992**, *97*, 6628.
6. Janoschek R., Weidemann E. G., Pfeiffer H., Zundel G.: *J. Am. Chem. Soc.* **1972**, *94*, 2378.
7. Zundel G.: *Trends Phys. Chem.* **1992**, *3*, 129.
8. Manahan S. E.: *Environmental Chemistry.*, Chap. 9, 7th ed. CRC Press LLC, Boca Raton 2000.
9. Wayne R. P.: *Chemistry of Atmospheres*, 3rd ed. Oxford University Press, New York 2000.
10. Rees M. H.: *Physics and Chemistry of the Upper Atmosphere*. Cambridge University Press, Cambridge 1989.
11. Hartley D. E., Villarin J. T., Black R. X., Davis C. A.: *Nature* **1998**, *391*, 471.
12. Lineberger W. C., Puckett L. J.: *Phys. Rev.* **1969**, *187*, 286.
13. Fehsenfeld F. C., Ferguson E. E.: *J. Geophys. Res., [Space Phys.]* **1969**, *74*, 2217.
14. Ferguson E. E., Fehsenfeld F. C.: *J. Geophys. Res., [Space Phys.]* **1969**, *74*, 5743.
15. Ferguson E. E., Fehsenfeld F. C., Albritton D. L. in: *Gas-Phase Ion Chemistry* (M. T. Bowers, Ed.), Vol. 1, p. 45. Academic Press, New York 1979.
16. Kopp E., Herrman U.: *Ann. Geophys.* **1984**, *2*, 83.
17. Mack P., Dyke J. M., Wright T. G.: *Chem. Phys.* **1997**, *218*, 243.
18. Hiraoka K., Yamabe S.: *J. Chem. Phys.* **1991**, *95*, 6800.
19. Choi J.-H., Kuwata K. T., Haas B.-M., Cao Y., Johnson M. S., Okumura M.: *J. Chem. Phys.* **1994**, *100*, 7153.
20. Asada T., Nagaoka M., Koseki S.: *Phys. Chem. Chem. Phys.* **2011**, *13*, 1590.
21. Dunkin D. B., Fehsenfeld F. C., Schmeltekopf E. E., Ferguson E. E.: *J. Chem. Phys.* **1971**, *54*, 3817.
22. Thomas L.: *Ann. Geophys.* **1983**, *1*, 61.
23. Keese R. G., Castleman J. A. W.: *Ann. Geophys.* **1983**, *1*, 75.
24. Arijs E.: *Ann. Geophys.* **1983**, *1*, 149.
25. Brasseur G., Chatel A.: *Ann. Geophys.* **1983**, *1*, 173.
26. Arijs E.: *Planet. Space Sci.* **1992**, *40*, 255.
27. Ye L., Cheng H.-P.: *J. Chem. Phys.* **1998**, *108*, 2015.
28. Wincel H.: *Chem. Phys. Lett.* **1998**, *292*, 193.
29. Wincel H.: *Int. J. Mass Spectrom.* **2000**, *203*, 93.
30. Gardner C.: *Geotimes* **2005**, *50*, 24.
31. Resende S. M., Pliego J. R., Vandresen S.: *Mol. Phys.* **2008**, *106*, 841.
32. Kotra J. P., Finnegan D. L., Zoller W. H., Hart M. A., Moyers J. L.: *Science* **1983**, *222*, 1018.
33. Seinfeld J. H., Pandis S. N.: *Atmospheric Chemistry and Physics – From Air Pollution to Climate Change*, 2nd ed. John Wiley and Sons, Inc., New York 2006.
34. Aiuppa A., Franco A., von Glasow R., Allen A. G., D'Alessandro W., Mather T. A., Pyle D. M., Valenza M.: *Atmos. Chem. Phys.* **2007**, *7*, 1441.
35. Hochstim A. R.: *Proc. Nat. Acad. Sci. U.S.A.* **1963**, *50*, 200.

36. Arnold S. T., Viggiano A. A., Morris R. A.: *J. Phys. Chem. A* **1997**, *101*, 9351.
37. Uhlár M., Pitonak M., Černušák I.: *Mol. Phys.* **2005**, *103*, 2309.
38. Uhlár M., Černušák I.: *Collect. Czech. Chem. Commun.* **2007**, *72*, 1122.
39. Becke A. D.: *Phys. Rev. A* **1988**, *38*, 3098.
40. Lee C., Yang W., Parr R. G.: *Phys. Rev. B* **1988**, *37*, 785.
41. Miehlich B., Savin A., Stoll H., Preuss H.: *Chem. Phys. Lett.* **1989**, *157*, 200.
42. Chai J. D., Head-Gordon M.: *Phys. Chem. Chem. Phys.* **2008**, *10*, 6615.
43. Chai J. D., Head-Gordon M.: *J. Chem. Phys.* **2008**, *128*, 15.
44. Bartlett R. J., Stanton J. F. in: *Reviews in Computational Chemistry* (K. B. Lipkowitz and D. B. Boyd, Eds), Vol. 5, p. 65. VCH Publishers, Inc., New York 1994;
45. Urban M., Noga J., Cole S. J., Bartlett R. J.: *J. Chem. Phys.* **1985**, *83*, 4041.
46. Urban M., Černušák I., Kellö V., Noga J.: *Methods in Computational Chemistry. Electron Correlation in Atoms and Molecules*, Vol. 1. Plenum Press, New York 1987.
47. Raghavachari K., Trucks G. W., Pople J. A., Headgordon M. L.: *Chem. Phys. Lett.* **1989**, *157*, 479.
48. Stanton J. F., Gauss J., Watts J. D., Nooijen M., Oliphant N., Perera S. A., Szalay P. G., Lauderdale W. J., Kucharski S. A., Gwaltney S. R., Beck S., Balkova A., Bernholdt D. E., Baeck K. K., Roczyczko P., Sekino H., Hober C., Bartlett R. J.: *ACES II*, A Program Product of the Quantum Theory Project. University of Florida, Gainesville (FL) 2007. Integral packages included are: VMOL (J. Almlöf and P. R. Taylor); VPROPS (P. Taylor); ABACUS (T. Helgaker, H. J. Aa. Jensen, P. Jørgensen, J. Olsen and P. R. Taylor).
49. Frisch M. J., Trucks G. W., Schlegel H. B., Scuseria G. E., Robb M. A., Cheeseman J. R., Scalmani G., Barone V., Mennucci B., Petersson G. A., Nakatsuji H., Caricato M., Li X., Hratchian H. P., Izmaylov A. F., Bloino J., Zheng G., Sonnenberg J. L., Hada M., Ehara M., Toyota K., Fukuda R., Hasegawa J., Ishida M., Nakajima T., Honda Y., Kitao O., Nakai H., Montgomery J. A., Jr., Peralta J. E., Ogliaro F., Bearpark M., Heyd J. J., Brothers E., Kudin K. N., Staroverov V. N., Kobayashi R., Normand J., Raghavachari K., Rendell A., Burant J. C., Iyengar S. S., Tomasi J., Cossi M., Rega N., Millam J. M., Klene M., Knox J. E., Cross J. B., Bakken V., Adamo C., Jaramillo J., Gomperts R., Stratmann R. E., Yazyev O., Austin A. J., Cammi R., Pomelli C., Ochterski J. W., Martin R. L., Morokuma K., Zakrzewski V. G., Voth G. A., Salvador P., Dannenberg J. J., Dapprich S., Daniels A. D., Farkas O., Foresman J. B., Ortiz J. V., Cioslowski J., Fox D. J.: *Gaussian 09*, Revision A.02. Gaussian, Inc., Wallingford (CT) 2009.
50. Dunning J. T. H.: *J. Chem. Phys.* **1989**, *90*, 1007.
51. Car R., Parrinello M.: *Phys. Rev. Lett.* **1985**, *55*, 2471.
52. VandeVondele J., Krack M., Mohamed F., Parrinello M., Chassaing T., Hutter J.: *Comput. Phys. Commun.* **2005**, *167*, 103.
53. Lippert G., Hutter J., Parrinello M.: *Theor. Chem. Acc.* **1999**, *103*, 124.
54. VandeVondele J., Hutter J.: *J. Chem. Phys.* **2007**, *127*.
55. Goedecker S., Teter M., Hutter J.: *Phys. Rev. B* **1996**, *54*, 1703.
56. Genovese L., Deutsch T., Neelov A., Goedecker S., Beylkin G.: *J. Chem. Phys.* **2006**, *125*, 074105.
57. Tuckerman M., Laasonen K., Sprik M., Parrinello M.: *J. Chem. Phys.* **1995**, *103*, 150.
58. Tuckerman M., Laasonen K., Sprik M., Parrinello M.: *J. Phys. Chem.* **1995**, *99*, 5749.
59. Marx D., Tuckerman M. E., Hutter J., Parrinello M.: *Nature* **1999**, *397*, 601.
60. Nonella M., Huber J. R., Ha T.-K.: *J. Phys. Chem.* **1987**, *91*, 5203.